Supporting information:

Journal: Journal of Materials Chemistry A

Title:

Solution-processable perylene diimide-based electron transport materials as non-fullerene alternatives for inverted perovskite solar cells

German Soto Perez,[a] Shyantan Dasgupta,[b,e] Wiktor Żuraw,[b] Rosinda Fuentes Pineda,[c] Konrad Wojciechowski,[b,c] Lethy Krishnan Jagadamma,[d] Ifor Samuel[d] and Neil Robertson*[a]

[a] School of Chemistry, Kings Buildings, University of Edinburgh, Edinburgh, EH9 3JJ, UK. E-mail: neil.robertson@ed.ac.uk.
[b] Saule Research Institute, Wroclaw PL 54-130, Poland.
[c] Saule Technologies, Wroclaw PL 54-427, Poland.
[d] Organic Semiconductor Centre, SUPA, School of Physics and Astronomy, University of St Andrews, St Andrews, KY16 9SS, UK.
[e] Faculty of Materials Engineering and Technical Physics, Poznan University of Technology Piotrowo 3, 60-965 Poznan, Poland.

Sample characterisation

Chemical characterisation of PDI was carried out using the following equipment: NMR spectroscopy was measured on a Bruker Avance spectrometer (500 MHz) with chemical shifts (δ) reported in ppm. Mass spectrometry was measured on a Micro-Tof through electrospray ionisation (ESI). UV-Vis absorption spectra were measured in a Jasco V-670 spectrophotometer. Solution characterisation was carried out in seven different solutions of each molecule (concentrations from $3.7x10^{-5}$ M to $3.7x10^{-6}$ M) prepared in $CHCl_3$ and measured in a 1 cm quartz cuvette at room temperature. Emission spectra were recorded in solution with a concentration of $9x10^{-4}$ M (~1mg/ml) using a Fluoromax-3 fluorometer. Electrochemical characterisation was measured with an Autolab type III potentiostat in an electrochemical cell composed of a platinum working electrode, platinum rod counter electrode and Ag/AgCl reference electrode. The electrochemical measurements were carried out in a 0.1 M solution of [TBA] [PF_6] in DCM purged with N_2 at room temperature. Ferrocene was used as an internal standard. Density Functional Theory (DFT) calculations were carried out using Gaussian 09 software with the hybrid B3LYP functional and the standard 6-31G(d) basis set, in vacuum conditions.

Figure S1 NMR Spectra

PDI-1

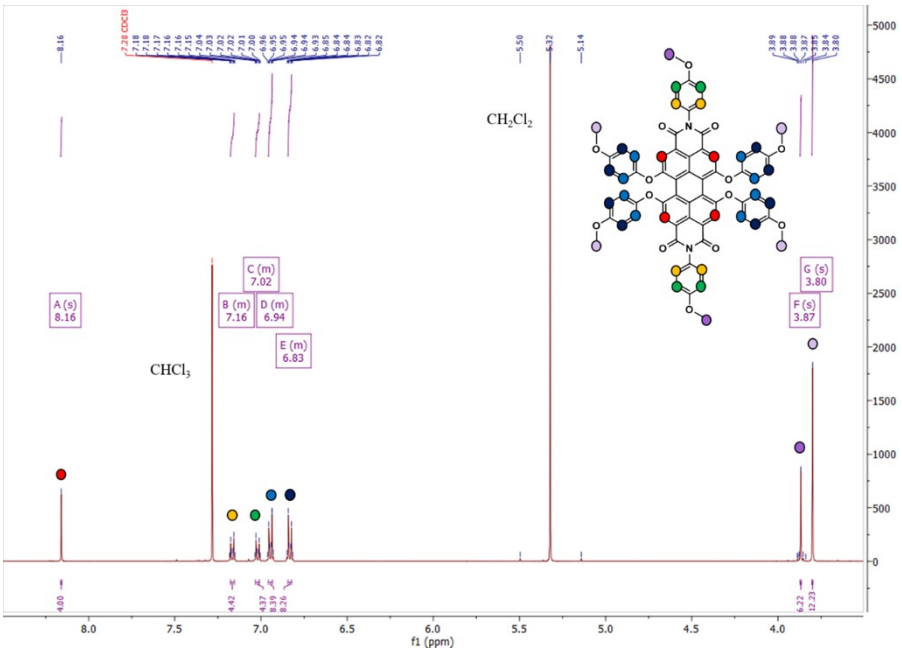

^{1}H NMR (500 MHz, Chloroform-d) δ 8.16 (s, 4H), 7.17 (d, J = 17.0 Hz, 4H), 7.04 – 7.00 (m, 4H), 6.96 – 6.93 (m, 8H), 6.85 – 6.81 (m, 8H), 3.87 (s, 6H), 3.80 (s, 12H).

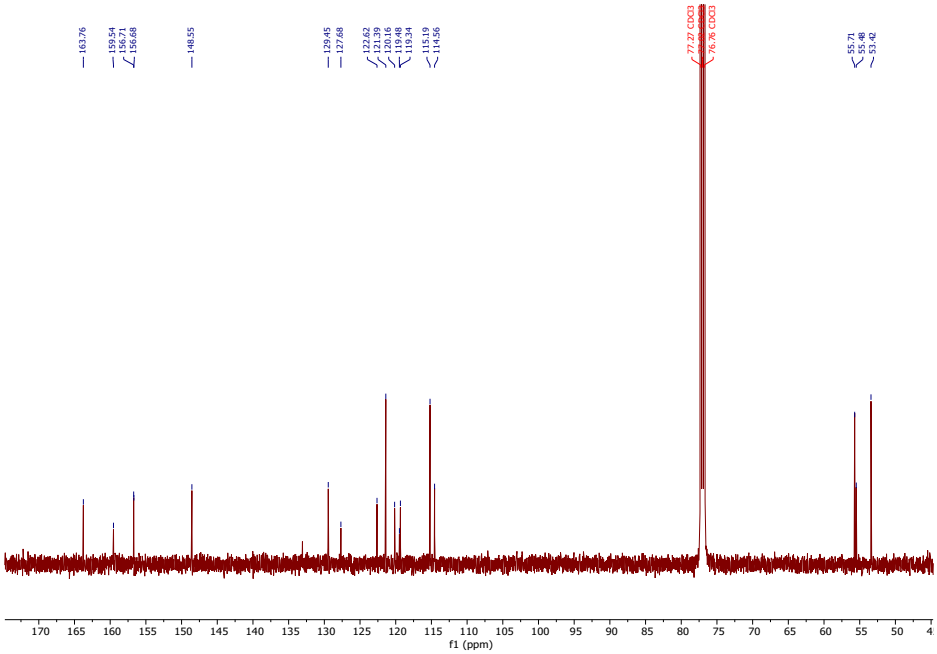

^{13}C NMR (126 MHz, Chloroform-d) δ 163.76, 159.54, 156.71, 156.68, 148.55, 129.45, 127.68, 122.62, 121.39, 120.16, 119.48, 119.34, 115.19, 114.56, 55.71, 55.48, 53.42.

PDI-2

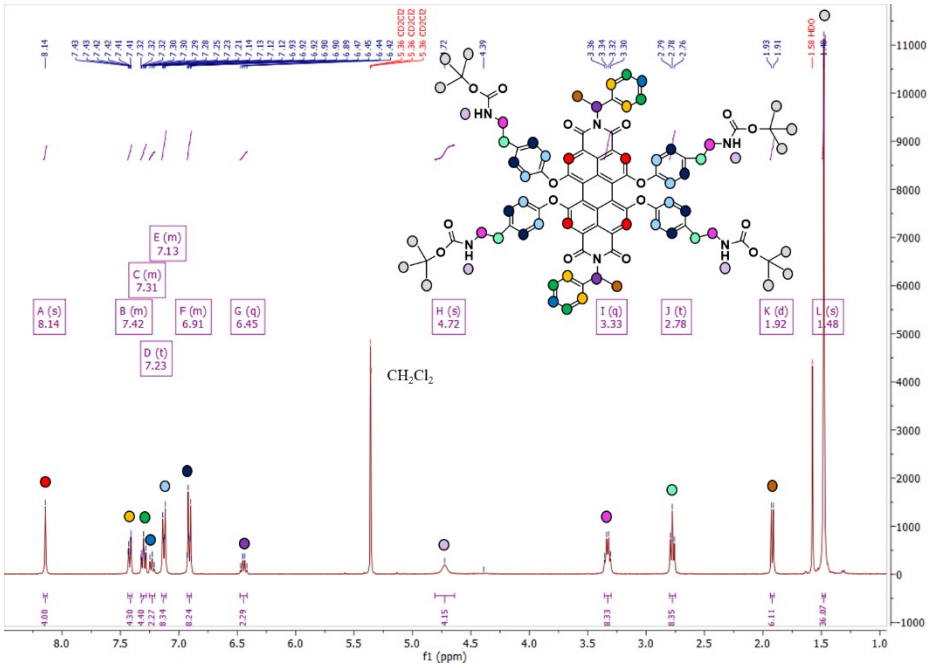

^{1}H NMR (400 MHz, Methylene Chloride-d2) δ 8.14 (s, 4H), 7.44 – 7.40 (m, 4H), 7.33 – 7.28 (m, 4H), 7.23 (t, J = 7.3 Hz, 2H), 7.15 – 7.11 (m, 8H), 6.93 – 6.89 (m, 8H), 6.45 (q, J = 7.0 Hz, 2H), 4.72 (s, 4H), 3.33 (q, J = 6.8 Hz, 8H), 2.78 (t, J = 7.1 Hz, 8H), 1.92 (d, J = 7.1 Hz, 6H), 1.48 (s, 36H).

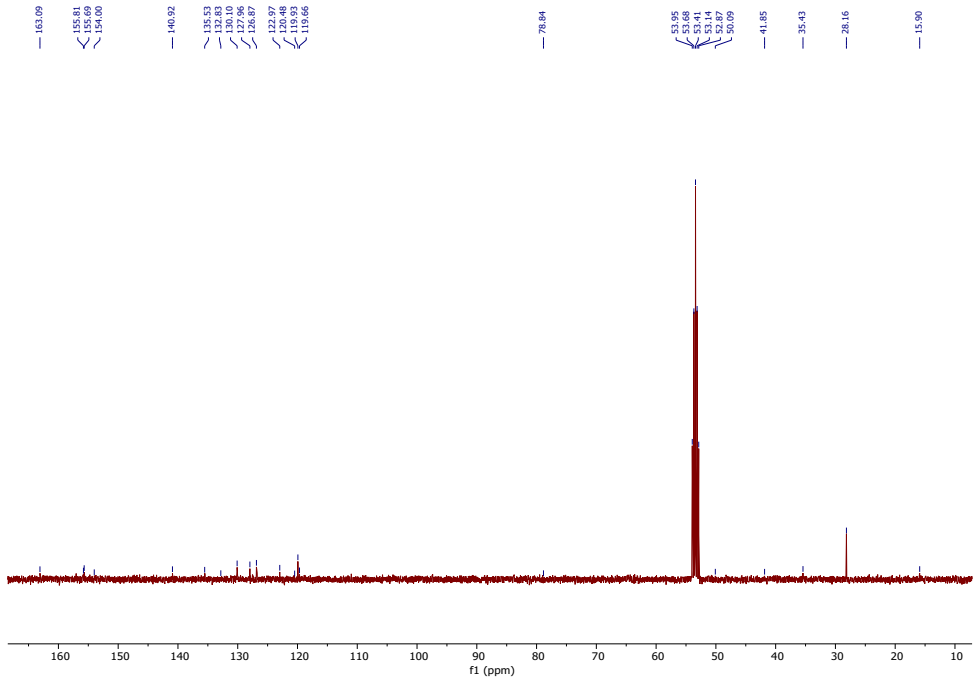

^{13}C NMR (126 MHz, Methylene Chloride-d2) δ 163.09, 155.81, 155.69, 154.00, 140.92, 135.53, 132.83, 130.10, 127.96, 126.87, 122.97, 120.48, 119.93, 119.66, 78.84, 52.87, 50.09, 41.85, 35.45, 28.16, 15.90.

PDI-3

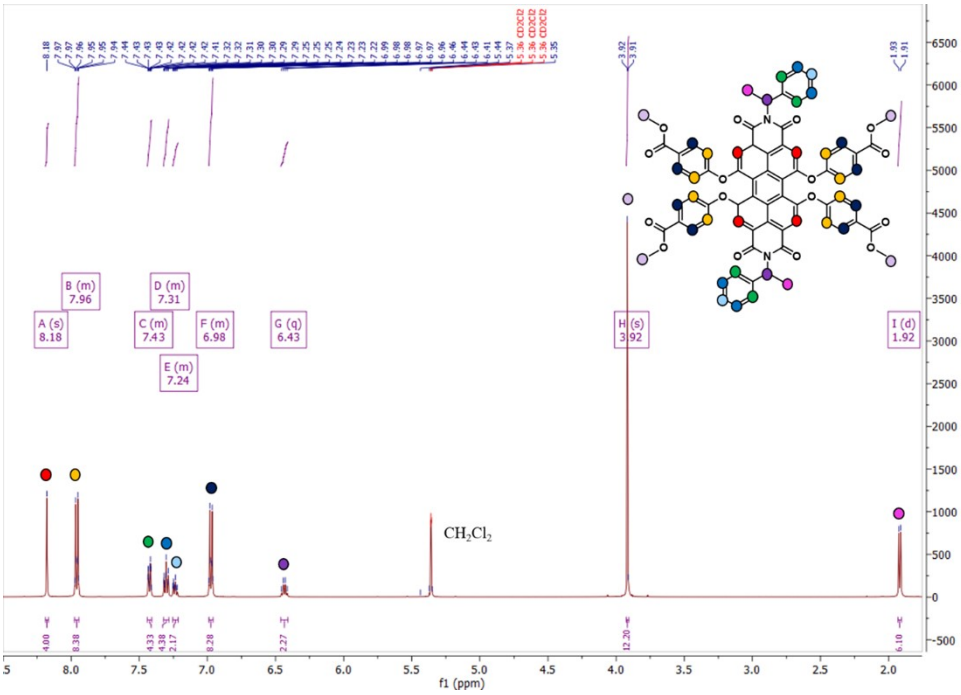

^{1}H NMR (500 MHz, Methylene Chloride-d2) δ 8.18 (s, 4H), 7.97 – 7.94 (m, 8H), 7.44 – 7.41 (m, 4H), 7.32 – 7.28 (m, 4H), 7.25 – 7.21 (m, 2H), 6.99 – 6.96 (m, 8H), 6.43 (q, J = 7.0 Hz, 2H), 3.92 (s, 12H), 1.92 (d, J = 7.1 Hz, 6H).

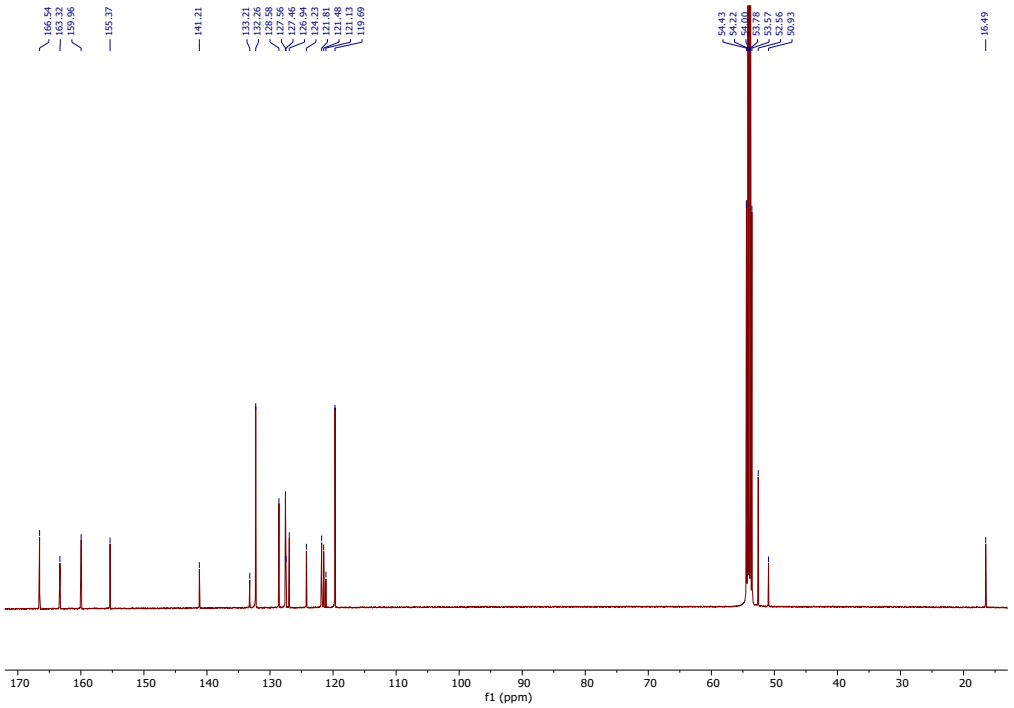

^{13}C NMR (126 MHz, Methylene Chloride-d2) δ 166.54, 163.32, 159.96, 155.37, 141.21, 133.21, 132.26, 128.58, 127.56, 127.46, 126.94, 124.23, 121.81, 121.48, 121.13, 119.69, 52.56, 50.93, 16.49.

Figure S2 Torsion calculation of PDI derivatives

Avogadro software was used to measure the twist of the PDI backbone, it was calculated as the average of the torsion angles between the carbons in both bay positions from the optimised geometry obtained by DFT.

PDI-1

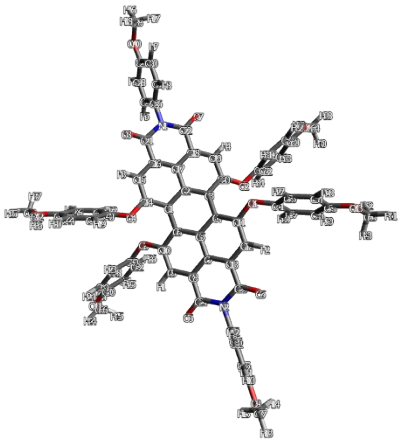

Torsion Properties

	Type	Atom 1	Atom 2	Atom 3	Atom 4	Torsion (°)
Torsion 29	COCH	C45	O12	C63	H36	61.6060
Torsion 122	COCH	C34	O9	C37	H14	61.2932
Torsion 104	HCOC	H17	C38	O10	C29	61.2147
Torsion 325	COCH	C50	O11	C66	H45	60.6108
Torsion 309	COCH	C60	O14	C64	H39	60.3236
Torsion 56	CCOC	C47	C40	O4	C14	50.3800
Torsion 152	CCCC	C14	C1	C6	C10	31.4927
Torsion 176	CCCC	C11	C4	C3	C20	31.2960
Torsion 61	COCC	C40	O4	C14	C15	28.8517
Torsion 153	CCCC	C2	C1	C6	C5	26.5480
Torsion 177	CCCC	C5	C4	C3	C2	26.3039
Torsion 69	COCC	C41	O1	C11	C12	20.3895
Torsion 272	CCOC	C19	C20	O2	C42	15.5190
Torsion 92	OCCC	O4	C14	C1	C6	15.0624
Torsion 107	OCCC	O1	C11	C4	C3	13.7262

PDI-2

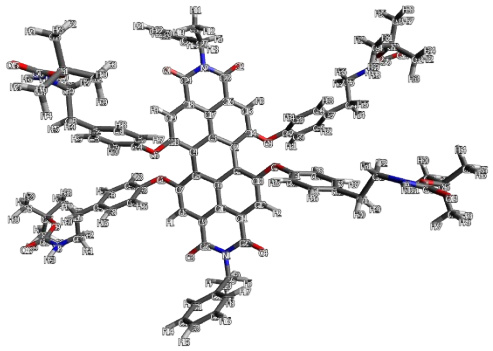

Torsion Properties

	Type	Atom 1	Atom 2	Atom 3	Atom 4	Torsion (°)
Torsion 513	HCNH	H46	C69	N4	H48	36.6948
Torsion 216	HCNH	H41	C66	N3	H43	36.5200
Torsion 182	COCC	C43	O5	C7	C8	36.0821
Torsion 112	COCC	C42	O8	C14	C15	34.5424
Torsion 94	CCCH	C36	C28	C27	H6	32.7031
Torsion 366	HCCC	H5	C25	C26	C35	31.4762
Torsion 202	CCCC	C14	C2	C1	C13	30.8197
Torsion 276	CCCC	C7	C5	C4	C20	30.5502
Torsion 460	CCCH	C61	C62	C71	H50	29.3959
Torsion 266	CCCH	C48	C47	C65	H40	27.7200
Torsion 203	CCCC	C3	C2	C1	C6	25.9736
Torsion 277	CCCC	C6	C5	C4	C3	25.9190
Torsion 479	CCCH	C53	C52	C68	H45	25.6592
Torsion 233	OCCC	O5	C7	C5	C4	15.6216
Torsion 143	OCCC	O8	C14	C2	C1	15.5513

PDI-3

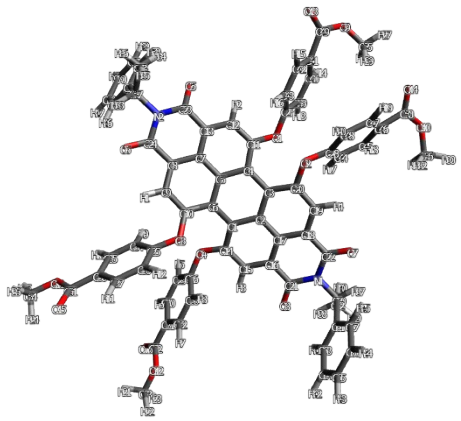

Torsion Properties

	Type	Atom 1	Atom 2	Atom 3	Atom 4	Torsion (°)
Torsion 337	COCC	C14	O4	C26	C33	50.3768
Torsion 61	CCOC	C34	C25	O3	C10	50.2071
Torsion 281	CCOC	C43	C27	O1	C11	42.4995
Torsion 78	COCC	C28	O2	C20	C19	39.3559
Torsion 77	COCC	C20	O2	C28	C44	36.6576
Torsion 254	CCOC	C12	C11	O1	C27	33.9093
Torsion 186	CCCC	C10	C6	C1	C14	31.1993
Torsion 171	CCCH	C67	C61	C60	H37	30.5425
Torsion 101	CCCC	C58	C57	C59	C72	30.2613
Torsion 200	CCCC	C20	C3	C4	C11	28.4942
Torsion 187	CCCC	C5	C6	C1	C2	26.3809
Torsion 323	CCOC	C15	C14	O4	C26	26.3088
Torsion 66	COCC	C25	O3	C10	C9	25.8759
Torsion 201	CCCC	C2	C3	C4	C5	25.2608
Torsion 238	CCCO	C6	C1	C14	O4	14.2054
Torsion 116	OCCC	O3	C10	C6	C1	14.1409

Figure S3 Beer-Lambert plot of PDI-1, -2 and -3

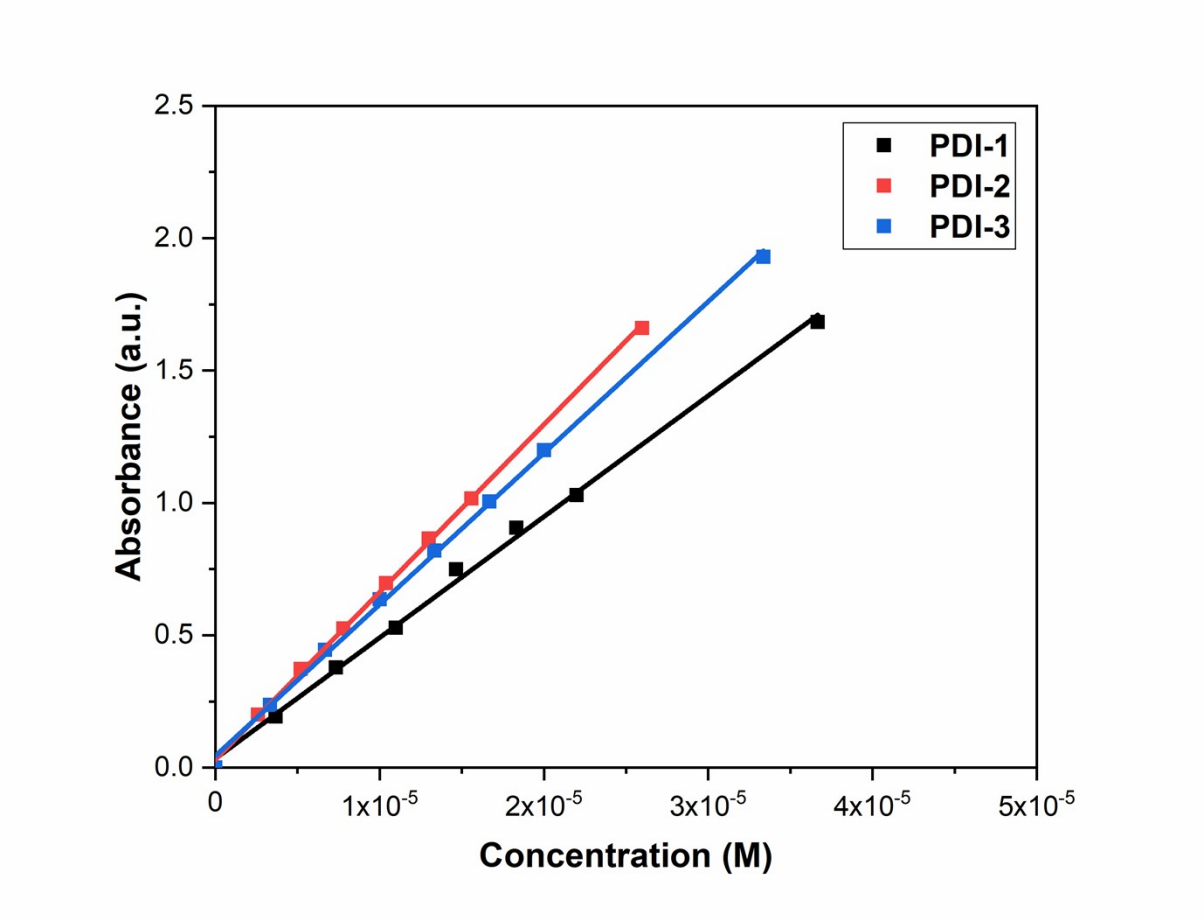

Figure S4 Charge mobility measurement of PDIs

The electron mobilities of PDI-1, -2 and -3, were investigated through the space-charge limited current (SCLC) technique. Samples were prepared as electron-only devices in a sandwich geometry with aluminium and ZnO electrodes on an ITO coated glass. Films were obtained by spin-coating PDI solutions (20 mg/ml in chlorobenzene) at 1,000 rpm for 60 s, and their thickness was measured with a Dektak profilometer; the final device had an ITO/ZnO/PDI/Al architecture. Electron injection was carried out through the Al electrode due to higher current density. The obtained J-V curves of each PDI plotted in logarithmic scale are shown in figure S4.

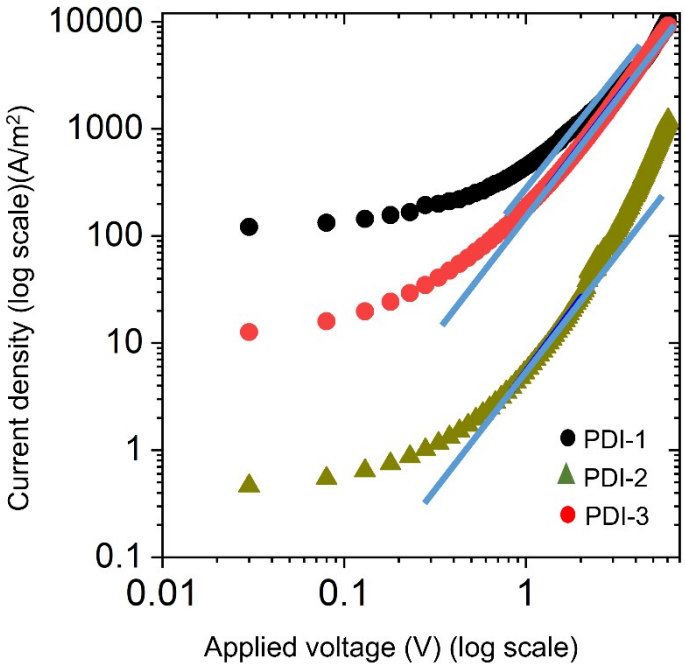

Figure S4 J-V characteristics of the electron-only devices prepared with PDI-1, -2 and -3.

Sample	Mobility [cm²/Vs]	Film thickness [nm]
PDI-1	3.8×10^{-5} ($\pm 1.6 \times 10^{-5}$)	63.6 (±5)
PDI-2	0.9×10^{-6} ($\pm 0.2 \times 10^{-6}$)	69 (±5)
PDI-3	1.6×10^{-5} ($\pm 3.2 \times 10^{-5}$)	72.7 (±5)

No evident trap-free regime was observed; therefore, the electron mobilities were estimated from the region of the curves where a straight line with an approximated slope of 2 could be fitted (depicted as the blue line on the curves). Such a region may be related to the trap-filling regime, in which the remaining traps within the material still hinder free charge mobility; however, it was not possible to clearly determine it was such a regime. From the obtained results, a tendency related to the size of the

substituents seems not only to play an important role in solubility but also in electron transport properties. PDI-1 with the less bulky substituent showed the highest mobility; in contrast, PDI-2 with the largest substituent showed the lowest mobility. Therefore, while solubility was gained for better processability, the electron mobility of the material in the solid state seems to be compromised to some extent.

Figure S5 Performance screen of PDI-based ETMs in inverted perovskite cells

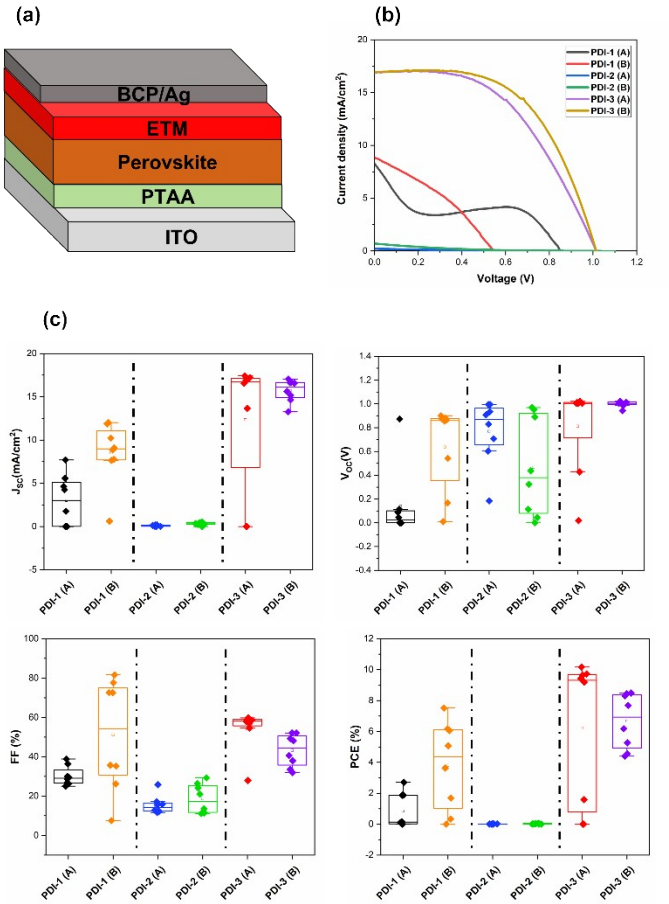

Figure S5. (a) Device architecture of inverted PSC on ITO-coated PET substrates. (b) J-V curves of best devices at different speed deposition, A and B represents 2,000 and 4,000 rpm, respectively. (c) Box plots of PV parameters over eight devices for each PDI.

Figure S6 Reverse and forward scan of champion devices with PCBM and PDI-based ETMs

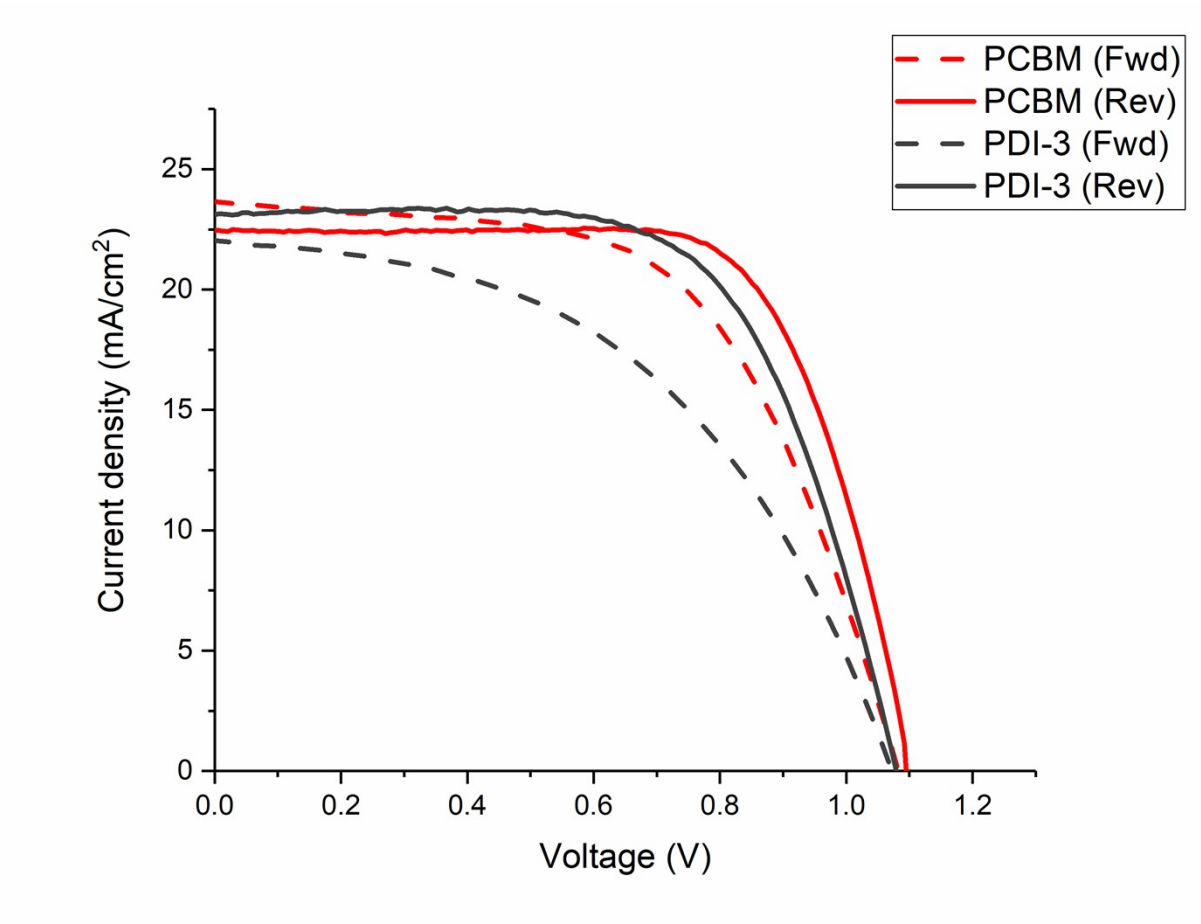

ETM	Scan	J_{sc} [mA/cm^2]	V_{oc} [V]	FF [%]	PCE [%]
PCBM	Reverse	22.46 (21.70)	1.09 (1.08)	71.5 (70.7)	17.30 (17)
	Forward	23.50 (22.97)	1.08 (1.07)	58.8 (57.6)	14.92 (14.56)
PDI-3	Reverse	23.02 (22.80)	1.08 (1.08)	67.5 (64.5)	16.80 (16.10)
	Forward	21.73 (21.13)	1.06 (1.04)	48.4 (45)	11.38 (11.16)